J. Fluid Mech. (1994), *vol.* 263, *pp.* 343–359

Interfacial instability due to MHD mode coupling in aluminium reduction cells

By A. D. SNEYD AND A. WANG
University of Waikato, Hamilton, New Zealand

(Received 13 November 1992 and in revised form 13 May 1993)

This paper analyses instabilities on the cryolite/aluminium interface in an aluminium reduction cell. The simplified cell model is a finite rectangular tank containing the two fluid layers, and carrying a uniform normal current. The magnetic field is assumed to be a linear function of position. Several previous studies have considered waves consisting of a single Fourier component but here we consider perturbations which are a general combination of the normal gravity-wave modes. We derive a system of coupled ordinary differential equations for the time-development of the mode amplitudes, and show that instability can occur via mode interactions, the electromagnetic perturbation force due to one mode feeding energy into the other. Growth rates are determined by computing the eigenvalues of an interaction matrix, and an approximate method using only the three leading diagonals is developed. If two modes have similar frequencies they may resonate and become unstable at a very low threshold current. We consider the influence of various cell parameters and draw some general conclusions about cell design.

1. Introduction

Aluminium is manufactured by electrolysis of aluminium oxide in Hall–Héroult cells in which a layer of electrolyte – or cryolite – about 4 cm deep, floats on a pool of liquid aluminium, typically about 20 cm deep. Current is passed into the cryolite via a carbon anode block and leaves the cell through the carbon cathode block, which acts as a container for the liquid metal. The oxygen which forms at the anode as a reduction by-product immediately combines with the carbon to form carbon dioxide which bubbles outward and eventually escapes from the cell. As the anode is thus burnt up it is continuously lowered and eventually replaced. Typical cell dimensions are about 8×4 m, and the DC current is about 2 or 3×10^5 A.

The intense current and associated magnetic field generate magnetohydrodynamic (MHD) forces which are useful in stirring the bath but which may also cause problems. One such is a deflection of the aluminium/cryolite interface from the horizontal, which in a new cell causes uneven current flow, current being diverted to the thinner sections of the cryolite layer (Lympany, Evans & Moreau 1983). However preferential burning of carbon where the current is strongest eventually carves out the anode block to follow the curvature of the aluminium surface. A more persistent problem occurs if the cryolite layer is too thin; gravity waves on the cryolite/aluminium interface can be destabilized by MHD effects, causing the aluminium to rise and short circuit with the anode. This problem limits cell efficiency since the thicker the cryolite layer (which offers most electrical resistance) the greater the cell resistance and power consumed.

One of the first theoretical accounts of the instability is by Urata (1985) who derives an approximate wave equation for the interface, which is widely used in industrial cell

modelling. A number of authors – Sneyd (1985, 1992, referred to below as paper I and paper II respectively), Moreau & Ziegler (1986), Pigny & Moreau (1991) – have analysed the linear stability of sinusoidal interfacial waves and concluded that the magnetic field distribution, cryolite layer depth, and aluminium pool depth are all important factors. This work has also provided insight into the physical mechanism driving the instability. Numerical modelling by Potočnik (1989) and Descloux, Flueck & Romerio (1991) has generally confirmed the theoretical conclusions.

In the above linear studies, a single Fourier component is considered. In a system where the various Fourier modes are *independent* – usually the case for a homogeneous system – stability can be determined by searching for the mode with the largest growth rate. An aluminium cell however is not homogeneous since spatial variation in the magnetic field $\boldsymbol{B}$ is implied by Ampère's law $\nabla \times \boldsymbol{B} = \mu_0 \boldsymbol{J}$. An interfacial perturbation consisting of a single Fourier component say $\exp(i\boldsymbol{k}\cdot\boldsymbol{x})$ gives rise to a current perturbation $\boldsymbol{j}$ also proportional to $\exp(i\boldsymbol{k}\cdot\boldsymbol{x})$. The resulting Lorentz force $\boldsymbol{j}\times\boldsymbol{B}(\boldsymbol{x})$ however comprises a spectrum of Fourier components which can supply energy to other Fourier modes.

In order to simplify the analysis as far as possible and highlight the essential physics we choose a very simple (and somewhat unrealistic) cell model in which the basic current $\boldsymbol{J}$ is purely vertical, and the basic field a linear function of position. Typically, when the cryolite/aluminium interface is perturbed, the restoring force due to gravity is much stronger than that due to electromagnetic effects. The resulting oscillation is therefore essentially a combination of normal gravity modes, weakly coupled by the electromagnetic force. We derive a *coupled* system of ordinary differential equations describing the time evolution of the amplitudes of the component gravity modes, and establish a simple approximate method of analysing stability. The key result is that destabilization can occur through a resonant interaction of two modes, the magnetic restoring force established by one mode feeding energy into the other. Thus the combination of two modes can be more unstable than either mode individually. The resonance effect is strongest if the natural frequencies of the modes are very similar, in which case destabilization may occur at a very low threshold current value.

The plan of the paper is as follows. In §2 we detail our reduction cell model and describe the unperturbed equilibrium. Then in §3 we consider a general interfacial disturbance and derive a system of coupled ordinary differential equations for the coefficients of its Fourier components. Stability is determined by the eigenvalues of a mode-coupling matrix, and §4 outlines the calculation of this matrix. In §5 we discuss a simple method of estimating stability which requires knowledge of only the three leading diagonals, and compare the approximate theory with exact numerical calculations. Results concerning the influence of various cell parameters are discussed in §6 and finally, §7 summarizes our conclusions.

2. Aluminium cell model

In a real cell the two-fluid layer (cryolite and liquid aluminium) is bounded laterally by the carbon cathode block and frozen cryolite, and vertically by the carbon anode block above and cathode block below (figure 1). In our model we take the lateral rigid boundary to be a cylinder of arbitrary cross-section. (In practice this cross-section will be rectangular, but the theory is easier to formulate generally and we later specialize to this particular case.) The carbon anode is bounded below by the plane $z = h_2$ and the carbon cathode above by $z = -h_1$, while $z = 0$ represents the unperturbed cryolite/aluminium interface (figure 1). The cryolite and aluminium volumes are

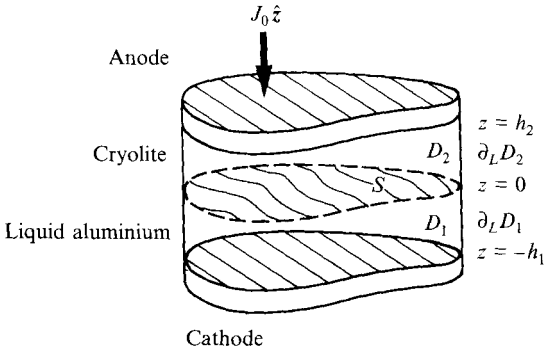

FIGURE 1. Diagram of model cell.

denoted by D_2 and D_1 respectively and their interface by S. The boundary of the region D_i is denoted by ∂D_i, and in particular the lateral surfaces by $\partial_L D_i$. Generally we use variables with a subscript i to label the particular form of the variable in D_i.

In the unperturbed state we take the electric current as purely vertical,

$$\boldsymbol{J} = J_0 \hat{\boldsymbol{z}},$$

and the magnetic field a linear function of position,

$$B_i = B_{0i} + \alpha_{ij} x_j \quad \text{or} \quad \boldsymbol{B} = \boldsymbol{B}_0 + \boldsymbol{B}_L,$$

where $\boldsymbol{B}_0$ is a constant vector and α_{ij} a constant second-order tensor. To avoid the complication of a steady-state electromagnetically driven flow we assume that the unperturbed Lorentz force is irrotational, which implies (paper I) that

$$\frac{\partial \boldsymbol{B}}{\partial z} = 0. \tag{2.1}$$

Equation (2.1) together with Maxwell's equations,

$$\nabla \cdot \boldsymbol{B} = 0, \quad \nabla \times \boldsymbol{B} = \mu_0 J_0 \hat{\boldsymbol{z}},$$

imply that α_{ij} must be of the form

$$\alpha_{ij} = J_0 \mu_0 \begin{pmatrix} 0 & -\frac{1}{2} & 0 \\ \frac{1}{2} & 0 & 0 \\ 0 & 0 & 0 \end{pmatrix} + J_0 \mu_0 \begin{pmatrix} R & Q & 0 \\ Q & -R & 0 \\ 0 & 0 & 0 \end{pmatrix},$$

where R and Q are constants (see paper I). The first antisymmetric term can be thought of as representing the rotational part $\boldsymbol{B}$ due to local currents, while the second symmetric term represents the irrotational field due to remote current sources, such as those in the bus bars. An alternative expression for α_{ij} can be written in terms of β – the angle between the x-axis and a principal axis of the second symmetric tensor:

$$\alpha_{ij} = J_0 \mu_0 \begin{pmatrix} 0 & -\frac{1}{2} & 0 \\ \frac{1}{2} & 0 & 0 \\ 0 & 0 & 0 \end{pmatrix} + J_0 \mu_0 q \begin{pmatrix} \cos\beta & \sin\beta & 0 \\ \sin\beta & -\cos\beta & 0 \\ 0 & 0 & 0 \end{pmatrix}. \tag{2.2}$$

The variable $q = (Q^2 + R^2)^{\frac{1}{2}}$ represents the ratio of the contribution to $\boldsymbol{B}$ from remote currents to that from the local current. Generally one would expect q to be of order unity.

The equilibrium Lorentz force can be balanced by a pressure gradient $-\nabla p_M$, where

$$p_M = J_0[\hat{z}\times(\boldsymbol{B}_0+\tfrac{1}{2}\boldsymbol{B}_L)]\cdot\boldsymbol{x}. \tag{2.3}$$

3. Normal mode analysis

3.1. *Normal mode decomposition*

We choose as our basis functions, the eigenfunctions $E_n(x,y), n = 1,2,\ldots$, of the eigenvalue problem

$$\nabla^2 E+\lambda^2 E = 0, \quad \nabla E\cdot\hat{\boldsymbol{n}} = 0 \quad \text{on} \quad \partial D_i. \tag{3.1a, b}$$

The eigenvalue corresponding to E_n is denoted by λ_n and we assume that these are in ascending order. The E_n satisfy the orthogonality relations

$$\int_S E_n E_m \,\mathrm{d}x\,\mathrm{d}y = \delta_{mn}\|E_n\|^2, \quad \int_S \nabla E_n\cdot\nabla E_m \,\mathrm{d}x\,\mathrm{d}y = \delta_{mn}\lambda_n^2\|E_n\|^2. \tag{3.2a, b}$$

The free-surface displacement $\eta(x,y)$ is expanded in terms of the E_n,

$$\eta = \sum_{n=1}^{\infty} a_n(t)\,E_n, \tag{3.3}$$

where the $a_n(t)$ are functions of time describing the evolution of the wave. We make the usual assumption of linear wave theory that η and hence the a_n coefficients are small.

An irrotational velocity field can be expanded in terms of the corresponding gravity-wave modes, $\boldsymbol{v}_n = \nabla\phi_n$ say, where the harmonic functions ϕ_n are defined by

$$\phi_{ni}(x,y,z) = G_{ni}(z)\,E_n(x,y), \tag{3.4}$$

and the functions $G_{in}(z)$ satisfy

$$G''_{ni}-\lambda_n^2 G_{ni} = 0, \quad G'_{n2}(h_2) = G'_{n1}(-h_1) = 0, \quad G'_{n2}(0) = G'_{n1}(0) = 1.$$

Specifically these functions are given by

$$G_{n2} = \frac{-\cosh[\lambda_n(h_2-z)]}{\lambda_n\sinh(\lambda_n h_2)}, \quad G_{n1} = \frac{\cosh[\lambda_n(h_1+z)]}{\lambda_n\sinh(\lambda_n h_1)}. \tag{3.5}$$

Note that

$$\nabla\phi_n\cdot\hat{\boldsymbol{n}} = 0 \quad \text{on} \quad \partial(D_1+D_2), \tag{3.6}$$

i.e. on the rigid lateral boundary, and also that

$$\frac{\partial\phi_{n1}}{\partial z} = \frac{\partial\phi_{n2}}{\partial z} = E_n \quad \text{at} \quad z = 0. \tag{3.7}$$

The linearized kinematic condition at the interface $z = 0$ is

$$\boldsymbol{v}_1\cdot\hat{\boldsymbol{z}} = \boldsymbol{v}_2\cdot\hat{\boldsymbol{z}} = \frac{\partial\eta}{\partial t}.$$

Substituting the expansion (3.3) for η we find

$$(\boldsymbol{v}_i\cdot\hat{\boldsymbol{z}})_{z=0} = \sum_{n=1}^{\infty}\dot{a}_n E_n,$$

so in view of (3.7) the expansion of $\boldsymbol{v}$ must take the form

$$\boldsymbol{v} = \sum_{n=1}^{\infty}\dot{a}_n\nabla\phi_n. \tag{3.8}$$

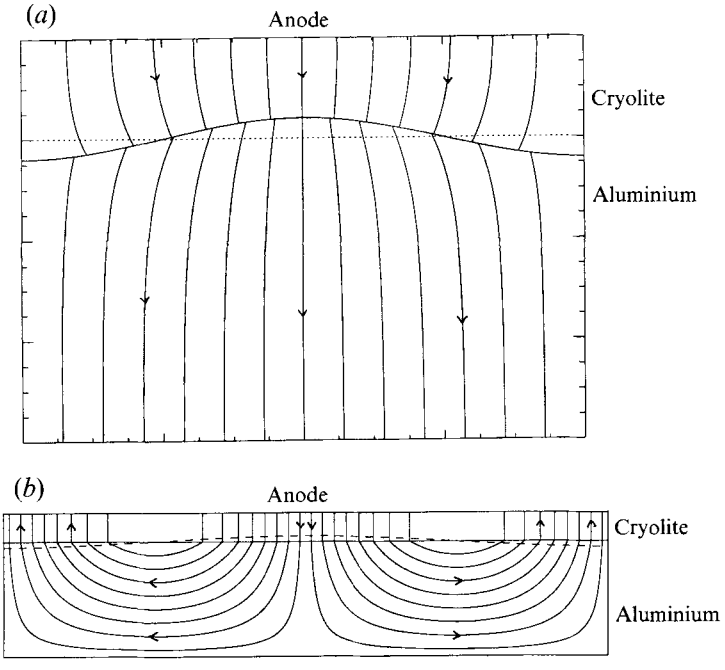

FIGURE 2. (*a*) Flow paths for total current J when cryolite layer is perturbed. (*b*) Streamlines of the current perturbation j.

In the case of pure gravity waves, the dynamic interface condition implies that the $a_n(t)$ satisfy the simple harmonic equation

$$\ddot{a}_n + \Omega_n^2 a_n = 0, \quad \Omega_n^2 = \frac{\lambda_n g \Delta\rho}{\rho_2 \mathscr{C}_{n2} + \rho_1 \mathscr{C}_{n1}},$$

where $\Delta\rho = \rho_1 - \rho_2$ and $\mathscr{C}_{ni} = \coth(\lambda_n h_i)$.

3.2. *Evolution equations*

Perturbation of the cryolite/aluminium interface diverts the electric current through the narrowest parts of the poorly conducting cryolite layer (figure 2*a*), and this current perturbation j leads to a perturbation f^M in the Lorentz force. In general f^M is rotational as must be the ensuing fluid motion v. Thus, in addition to the irrotational velocity field (3.8) there will be a rotational circulation v_R say, and we write

$$v = \sum_{n=1}^{\infty} \dot{a}_n \nabla\phi_n + v_R \quad \text{or} \quad v = v_P + v_R \quad \text{say.} \tag{3.9}$$

In general such a decomposition of v into rotational and irrotational components would not be unique, but since the potential flow v_P is solenoidal and satisfies all the required boundary conditions, it follows that

$$\nabla \cdot v_R = 0, \quad v_R \cdot \hat{n} = 0 \quad \text{on} \quad \partial D_i. \tag{3.10}$$

The conditions (3.10) ensure the uniqueness of the decomposition.

The linearized equation of motion in each layer is

$$\rho_i \frac{\partial v_i}{\partial t} = -\nabla p_i - \rho_i g \hat{z} + f_i^M, \tag{3.11}$$

where the unperturbed Lorentz force and its balancing pressure gradient (see (2.3)) have been omitted.

Evolution equations for the coefficients $a_n(t)$ are obtained by taking the inner product of the equation of motion (3.11) with each $\nabla\phi_k$. We write the inner product of two vector fields $\boldsymbol{f}, \boldsymbol{g}$, i.e.

$$\int_{D_1+D_2} \boldsymbol{f}\cdot\boldsymbol{g}\,\mathrm{d}V \quad \text{more simply as} \quad \langle \boldsymbol{f}, \boldsymbol{g}\rangle.$$

To deal with the first term of (3.11) we note that

$$\langle \boldsymbol{v}_R, \nabla\phi_k\rangle = \int_{D_1+D_2} \nabla\cdot(\phi_k \boldsymbol{v}_R)\,\mathrm{d}V = \int_{\partial D_1+\partial D_2} \phi_k \boldsymbol{v}_R\cdot\hat{\boldsymbol{n}} = 0,$$

in view of conditions (3.10). Fortunately the rotational circulation (which would be awkward to calculate) does not affect the evolution equations.

To deal with the potential flow component $\boldsymbol{v}_P$ we use expansion (3.8) and the orthogonality condition (3.2*b*). Then applying the divergence theorem to $\nabla\phi_k\cdot\nabla\phi_k = \nabla\cdot(\phi_k\nabla\phi_k)$, and the boundary conditions (3.6), (3.7) we find,

$$\langle \rho\nabla\phi_k, \nabla\phi_k\rangle = \sum_{i=1}^{2}\int_{D_i} \rho_i \nabla\phi_{ki}\cdot\nabla\phi_{ki}\,\mathrm{d}V = \int_S (\rho_1\phi_{k1}-\rho_2\phi_{k2})_{z=0} E_k\,\mathrm{d}x\,\mathrm{d}y.$$

Since the velocity $\boldsymbol{v}^P$ is a small perturbed quantity, the integral is taken across the unperturbed interface $z = 0$. Using (3.5) we now find

$$\langle \rho\dot{\boldsymbol{v}}_P, \nabla\phi_k\rangle = \frac{\ddot{a}_k}{\lambda_k}(\rho_2\mathscr{C}_{k2}+\rho_1\mathscr{C}_{k1})\|E_k\|^2. \tag{3.12}$$

Since $-\nabla p_i\cdot\nabla\phi_{ki} = -\nabla\cdot(p\nabla\phi_{ki})$, the inner product of $\nabla\phi_k$ with the pressure term in (3.11) yields

$$\langle -\nabla p, \nabla\phi_k\rangle = \int_{S'} p_{S'}(\nabla\phi_{k2}-\nabla\phi_{k1})\cdot\hat{\boldsymbol{n}}\,\mathrm{d}S. \tag{3.13}$$

Here S' represents the perturbed interface, and we have made use of the fact that p is continuous across the interface, the common value being denoted by $p_{S'}$. We may write $p_{S'} = p_0+p'$ where p_0 is the constant value of the unperturbed pressure on the unperturbed interface $z = 0$, and p' a small perturbation. Then to leading order (3.13) becomes

$$p_0\int_{S'}(\nabla\phi_{k2}-\nabla\phi_{k1})\cdot\hat{\boldsymbol{n}}\,\mathrm{d}S+\int_S p'(\nabla\phi_{k2}-\nabla\phi_{k1})\cdot\hat{\boldsymbol{z}}\,\mathrm{d}S = 0.$$

The first term vanishes by virtue of mass conservation of each layer, and the second by (3.7). Thus

$$\langle -\nabla p, \nabla\phi_k\rangle = 0. \tag{3.14}$$

This expresses the simple physical result that pressure forces do no net work.

In evaluating the inner product of $\nabla\phi_k$ with the gravity term, the first-order contribution arises from the perturbation to the region of integration, $\eta\,\mathrm{d}S$ having been added to D_1 and removed from D_2. Thus,

$$\begin{aligned}\langle \rho g\hat{\boldsymbol{z}}, \nabla\phi_k\rangle &= \int_S -gE_k\Delta\rho\eta\,\mathrm{d}S \\ &= -g\Delta\rho a_k\|E_k\|^2,\end{aligned} \tag{3.15}$$

by virtue of the orthogonality condition (3.2*a*).

Since f_i^M is a linear function of η (the exact relationship is detailed in §4) then from (3.3) we see that

$$f_i^M = \sum_{n=1}^{\infty} a_n(t) f_{ni}^M, \tag{3.16}$$

where f_{ni}^M represents the (linearized) contribution to the Lorentz force perturbation arising from a perturbation E_n to the free surface. We define dimensionless magnetic interaction coefficients γ_{kn} by setting

$$\gamma_{kn} = \frac{\lambda_1}{m_0 J_0^2 \|E_k\|^2} \langle \nabla\phi_k, f_{ni}^M \rangle, \tag{3.17}$$

and it follows from (3.16) that

$$\langle f_M, \nabla\phi_k \rangle = \frac{\mu_0 J_0^2}{\lambda_1} \|E_k\|^2 \sum_{n=1}^{\infty} \gamma_{kn} a_n(t). \tag{3.18}$$

Now combining the results (3.12), (3.14), (3.15), (3.18), and taking the inner product of (3.11) with $\nabla\phi_k$ we obtain the following set of evolution equations:

$$\ddot{a}_k + \Omega_k^2 \left(a_k - \epsilon \sum_{n=1}^{\infty} \gamma_{kn} a_n \right) = 0. \tag{3.19}$$

The dimensionless parameter

$$\epsilon = \frac{\mu_0 J_0^2}{g \lambda_1 \Delta\rho} \tag{3.20}$$

is a measure of the relative importance of magnetic and gravity restoring forces to interfacial waves. In a typical aluminium reduction cell, ϵ is quite small – of order 10^{-1} or 10^{-2}.

4. Calculation of γ_{kn}

The γ_{kn} coefficients represent the potentially destabilizing feedback of the Lorentz force perturbation f_i^M. To leading order,

$$f_i^M = \boldsymbol{j}_i \times \boldsymbol{B} + J_0 \hat{\boldsymbol{z}} \times \boldsymbol{b}_i, \tag{4.1}$$

where the $\boldsymbol{j}_i$ is the current perturbation.

4.1. *Current perturbation*

In calculating the current perturbation $\boldsymbol{j}_i$ we shall for simplicity treat the anode as a single uniform carbon block. Many modern plants use a series of slightly separated anodes, so that the $\boldsymbol{j}_i$ circuit is completed in the buswork, leading to a different magnetic field perturbation.

Using Ohm's law and the electrostatic approximation, we write

$$\boldsymbol{j}_i = \nabla\psi_i, \quad \nabla^2\psi_i = 0. \tag{4.2a, b}$$

The lateral cell boundaries have much weaker electrical conductivity than the interior, so we may treat them as insulating and set

$$\frac{\partial\psi_i}{\partial n} = \boldsymbol{j}_i \cdot \hat{\boldsymbol{n}} = 0 \quad \text{on} \quad \partial_L D_i. \tag{4.3}$$

Thus, the general form for the current potential perturbation can be expanded in the form

$$\psi_i = J_0 \sum_{n=1}^{\infty} H_{ni}(z)\, a_n(t)\, E_n(x, y), \tag{4.4}$$

where the $H_{ni}(z)$ satisfy $$H''_{ni}(z) - \lambda_n^2 H_{ni}(z) = 0. \tag{4.5}$$

One can take advantage of the electrical conductivity ordering,

$$\sigma_{cryolite} \ll \sigma_{carbon} \ll \sigma_{aluminium},$$

to derive approximate boundary conditions for the H_{in}. Since the carbon anode is a perfect conductor relative to the cryolite, and the carbon cathode a perfect insulator in comparison with liquid aluminium, we may approximate

$$H_{n2}(h_2) = 0, \quad H'_{n1}(-h_1) = 0. \tag{4.6a, b}$$

Continuity of tangential electric field and normal current at $z = 0$ gives

$$H_{n2}(0) + 1 = 0, \quad H'_{n1}(0) = H'_{n2}(0). \tag{4.7a, b}$$

(A detailed justification of these approximate boundary conditions is given in the appendix to paper II.) Explicitly one finds

$$H_{n2}(z) = -\frac{\sinh \lambda_n (h_2 - z)}{\sinh \lambda_n h_2}, \quad H_{n1}(z) = \mathscr{C}_{n2} \frac{\cosh \lambda_n (h_1 + z)}{\sinh \lambda_n h_1}. \tag{4.8}$$

4.2. *Orders of magnitude*

In a typical aluminium reduction cell, the layer depths h_2, h_1 are typically about 5 cm and 20 cm respectively – much less that the horizontal lengthscale, L say, of several metres. This large aspect ratio intensifies the perturbation currents, particularly in the aluminium layer, and we need to estimate $|\boldsymbol{j}|$ to identify the dominant terms in perturbed electromagnetic body force.

In view of the large aspect ratio, the terms $\lambda_n h_i$ or $\lambda_n z$ in (4.8) will be small. Thus we can approximate

$$H_{n2}(z) \approx -(1 - z/h_2), \quad H_{n1} \approx 1/(\lambda_n^2 h_1 h_2),$$

and the dominant components of the perturbation currents are given by

$$\boldsymbol{j}_2 = \frac{J_0 \eta}{h_2} \hat{\boldsymbol{z}}, \quad \boldsymbol{j}_1 = \frac{J_0}{h_1 h_2} \sum_{n=1}^{\infty} \lambda_n^{-2} a_n(t)\, \nabla E_n. \tag{4.9}$$

In the cryolite $\boldsymbol{j}$ is almost vertical, as the current follows the shortest path through the poorly conducting layer. Where the layer is narrow ($\eta > 0$) $\boldsymbol{j}_2$ reinforces $J_0 \hat{\boldsymbol{z}}$ since current converges towards this region. In the aluminium $\boldsymbol{j}_1$ is intense and nearly horizontal as the current is forced to recirculate through the narrow layer. Field lines of the current perturbation $\boldsymbol{j}$ are shown in figure 2(*b*).

The perturbation current is most intense in the aluminium, where

$$|\boldsymbol{j}| = O\left(\frac{J_0 AL}{h_1 h_2}\right), \tag{4.10}$$

A being a typical free-surface elevation and L a horizontal lengthscale: $L = \lambda_1^{-1}$ for example. The ratio of the electromagnetic force perturbation to the gravity body force perturbation is of order

$$\frac{jB}{g\Delta\rho A/L} = \frac{\mu_0 J_0^2 L^3}{g\Delta\rho h_1 h_2} = N_M \quad \text{say}, \tag{4.11}$$

where $B = \mu_0 J_0 L$ is a typical magnetic field strength. Taking typical values in SI units, $J_0 = 10^4$, $\Delta\rho = 1.82 \times 10^2$, $g = 9.81$, $L = 2$, $h_1 = 2 \times 10^{-1}$, $h_2 = 5 \times 10^{-2}$, we find

$$N_M = 56.3.$$

It therefore appears that electromagnetic forces dominate the evolution of the perturbation. Current intensification due to the large cell aspect ratio means that the correct ratio of electromagnetic to gravity forces is not ϵ (defined in (3.20)), but rather

$$N_M = \epsilon \frac{L^2}{h_1 h_2}. \tag{4.12}$$

4.3. *Magnetic field perturbation*

The magnetic perturbation $\boldsymbol{b}_{ni}$ due to mode n of the current perturbation satisfies

$$\nabla \cdot \boldsymbol{b}_{ni} = 0, \quad \nabla \times \boldsymbol{b}_{ni} = \mu_0 J_0 a_n(t) \nabla [H_{ni}(z) E_n]. \tag{4.13a, b}$$

As a trial solution we set $\boldsymbol{b}_{ni} = \mu_0 J_0 \nabla \chi_{ni} \times \hat{\boldsymbol{z}}$.

This satisfies (4.13*a*) identically, and substitution into (4.13*b*) gives

$$\nabla \times \boldsymbol{b}_{ni} = \mu_0 J_0 \nabla \left(\frac{\partial \chi_{ni}}{\partial z} \right).$$

Using (4.5) we see that (4.13*b*) will be satisfied by choosing $\chi_{ni} = \lambda_n^{-2} H'_{ni}(z) E_n(x, y)$. Thus, the magnetic perturbation is

$$\boldsymbol{b}_i = \mu_0 J_0 \sum_{n=0}^{\infty} \frac{a_n(t)}{\lambda_n^2} H'_{ni}(z) \nabla E_n(x, y) \times \hat{\boldsymbol{z}}. \tag{4.14}$$

The current perturbation extends of course into both the anode and cathode where it is also given by potentials of the form (4.4), which we have not quoted explicitly since this has no effect on the cell dynamics. Expressions of the form (4.14) could also be written for the field perturbation in anode and cathode, and we note that $\boldsymbol{b}$ is continuous across the interfaces $z = h_2$, $z = 0$, $z = -h_1$, since H'_{ni} is continuous by virtue of continuity of normal current. However, our solution (4.14) is not continuous across the lateral boundaries where, in view of (3.1*b*), $\nabla E_n = (\partial E_n / \partial s) \hat{\boldsymbol{s}}$, s being a coordinate along the boundary. The field perturbation at this boundary is therefore given by

$$(\boldsymbol{b}_i)_{\partial_L D_i} = \mu_0 J_0 \sum_{n=1}^{\infty} \frac{a_n(t)}{\lambda_n^2} H'_{ni}(z) \frac{\partial E_n}{\partial s} \hat{\boldsymbol{n}}.$$

To make the field continuous across $\partial_L D$ we superimpose a potential magnetic field $\boldsymbol{b}^P$ say, due to a surface distribution of 'magnetic charge' of strength $(\boldsymbol{b} \cdot \hat{\boldsymbol{n}})_{\partial_L D}$ on $\partial_L D$. Strictly speaking therefore, the field $\boldsymbol{b}^P$ should be added to our solution (4.14). However, the dominant contribution to this field arises from the intense horizontal current in the aluminium, so in the cell interior $\boldsymbol{b}_P$ will be $O(h_1 \boldsymbol{b}/L)$ and hence negligible for a typical high-aspect-ratio cell.

From (4.14) one can find the order of magnitude estimate of the perturbation field,

$$|\boldsymbol{b}| = O\left(\frac{\mu_0 J_0 AL}{h_2} \right). \tag{4.15}$$

This estimate can be deduced directly from Ampère's law, $\nabla \times \boldsymbol{b} = \mu_0 \boldsymbol{j}$ together with (4.10), using the lengthscale h_1 for derivatives of $\boldsymbol{b}$.

4.4. *Lorentz force perturbation*

Substituting (4.4) and (4.14) into (4.1), one finds the Lorentz force perturbation

$$\boldsymbol{f}_n^M = \frac{\mu_0 J_0^2}{\lambda_n^2} H_n' \nabla E_n \times \hat{\boldsymbol{z}} + J_0 (H_n \nabla E_n + H_n' E_n \hat{\boldsymbol{z}}) \times \boldsymbol{B}.$$

Thus,

$$\boldsymbol{f}_n^M \cdot \nabla \phi_k = \frac{\mu_0 J_0^2}{\lambda_n^2} H_n' G_k \nabla E_k \cdot \nabla E_n + J_0 G_k H_n (\nabla E_n \times \boldsymbol{B}) \cdot \nabla E_k$$
$$+ J_0 H_n G_k' E_k (\nabla E_n \times \boldsymbol{B}) \cdot \hat{\boldsymbol{z}} - J_0 H_n' G_k E_n (\nabla E_k \times B) \cdot \hat{\boldsymbol{z}}. \quad (4.16)$$

Substituting (4.16) into (3.17), yields

$$\gamma_{kn} = \delta_{kn} \lambda_1 I_{kk}^{(1)} + \frac{\lambda_1}{\mu_0 J_0 \| E_k \|^2} [B_{0z} I_{kn}^{(0)} I_{kn}^{(3)} + I_{kn}^{(2)} I_{kn}^{(4)} - I_{kn}^{(1)} I_{nk}^{(4)}], \quad (4.17)$$

where

$$I_{kn}^{(0)} = \int_{-h_1}^{h_2} G_k(z) H_n(z) \, \mathrm{d}z, \quad (4.18a)$$

$$I_{kn}^{(1)} = \int_{-h_1}^{h_2} G_k(z) H_n'(z) \, \mathrm{d}z, \quad I_{kn}^{(2)} = \int_{-h_1}^{h_2} G_k'(z) H_n(z) \, \mathrm{d}z, \quad (4.18b, c)$$

$$I_{kn}^{(3)} = \int_S (\nabla E_k \times \nabla E_n) \cdot \hat{\boldsymbol{z}} \, \mathrm{d}x \, \mathrm{d}y, \quad I_{kn}^{(4)} = \int_S E_k (\nabla E_n \times \boldsymbol{B}) \cdot \hat{\boldsymbol{z}} \, \mathrm{d}x \, \mathrm{d}y. \quad (4.18d, e)$$

In the particular case of most interest, the rectangular cell, $0 \leqslant x \leqslant a$, $0 \leqslant y \leqslant b$ the eigenfunctions are given by

$$E_k = \cos \frac{m\pi x}{a} \cos \frac{n\pi y}{b},$$

where m, n range over the positive integers and

$$\lambda_k = \left[\left(\frac{m\pi}{a} \right)^2 + \left(\frac{n\pi}{b} \right)^2 \right]^{\frac{1}{2}}.$$

Expressions for the integrals $I_{kn}^{(j)}$ in this case are given in the Appendix.

4.5. *Rescaling the interaction coefficients*

The discussion of orders of magnitude earlier in this section showed that the dimensionless parameter ϵ underestimates the perturbed electromagnetic force. Equation (4.12) shows that in order to obtain interaction coefficients Γ_{kn} of order unity we should rescale by setting

$$\Gamma_{kn} = \lambda_1^2 h_1 h_2 \gamma_{kn} \quad \text{so that} \quad \epsilon \gamma_{kn} = N_M \Gamma_{kn}. \quad (4.19a, b)$$

Equation (3.19) can now be rewritten

$$\ddot{a}_k + \Omega_k^2 \left(a_k - N_M \sum_{n=1}^{\infty} \Gamma_{kn} a_n \right) = 0. \quad (4.20)$$

It follows from (4.19a) and (4.17) that

$$\Gamma_{kn} = \delta_{kn} h_1 h_2 \lambda_1^3 I_{kk}^{(1)} + \frac{\lambda_1^3 h_1 h_2}{\mu_0 J_0 \| E_k \|^2} [B_{0z} I_{kn}^{(0)} I_{kn}^{(3)} + I_{kn}^{(2)} I_{kn}^{(4)} - I_{kn}^{(1)} I_{nk}^{(4)}]. \quad (4.21)$$

Order-of-magnitude estimates show that the second term in this equation is $O(1)$ while the remaining terms are $O(h_1/L)$. Thus the vertical component of magnetic field seems to have a dominant influence, and this is confirmed by our detailed results described in §6. However, the horizontal fields may sometimes be much larger than B_{0z} so we retain all terms in (4.21). The neglected term $\boldsymbol{b}_P$ in the perturbed magnetic field would give a contribution to Γ_{kn} of order $(h_1/L)^2$.

5. Approximate analysis for slightly separated natural frequencies

If we truncate the infinite system (4.20) to size N and let $a_n(t) = x_n \mathrm{e}^{\mathrm{i}\omega t}$, we find that ω^2 must be an eigenvalue of the matrix, $\boldsymbol{\Omega} - N_M \boldsymbol{\Gamma}$, where

$$\boldsymbol{\Omega} = \mathrm{diag}(\Omega_1^2, \Omega_2^2, \ldots, \Omega_N^2), \quad \boldsymbol{\Gamma} = (\Gamma_{ij}).$$

The constants x_n form the corresponding eigenvector. Any eigenvalue with non-zero imaginary part, $\omega^2 = \sigma + \mathrm{i}\tau$, say, where σ and τ are real, corresponds to an unstable mode with growth rate $\{\frac{1}{2}[(\sigma^2+\tau^2)^{\frac{1}{2}} + \sigma]\}^{\frac{1}{2}}$.

When $N_M = 0$ (no electromagnetic effects) the eigenvalues are simply the natural frequencies for gravity waves in the cavity, which are always stable provided $\rho_2 < \rho_1$. However, as N_M increases, a pair of real eigenvalues may coalesce and bifurcate into a complex-conjugate pair (figure 3*a*). Clearly if two natural frequencies are close together bifurcation – and hence instability – may occur at a small value of N_M, in which case a simple approximate stability criterion can be established.

Suppose (without loss of generality) that the natural frequencies Ω_1, Ω_2 are close together. The eigenvalue equation can be written,

$$\begin{pmatrix} \boldsymbol{A}_1 & \boldsymbol{B}_1^T \\ \boldsymbol{B}_2 & \boldsymbol{A}_2 \end{pmatrix} \begin{pmatrix} V_1 \\ V_2 \end{pmatrix} = \omega^2 \begin{pmatrix} V_1 \\ V_2 \end{pmatrix},$$

where $\boldsymbol{A}_1$ is 2×2, $\boldsymbol{B}_1$ and $\boldsymbol{B}_2$ $(N-2) \times 2$, etc. The first two rows of this equation give

$$\boldsymbol{A}_1 V_1 + \boldsymbol{B}_1^T V_2 = \omega^2 V_1, \tag{5.1}$$

where the matrix $\boldsymbol{B}_1 = O(N_M)$ since it is composed entirely of elements of $N_M \boldsymbol{\Gamma}$. When $N_M = 0$ the eigenvector associated with Ω_1 or Ω_2 is $(1,0,0,\ldots)^T$, or $(0,1,0,\ldots)^T$, or a linear combination of both in the case of a repeated eigenvalue. Thus the vector V_2 is also $O(N_M)$ and (5.1) can be written,

$$\boldsymbol{A}_1 V_1 = \omega^2 V_1 + O(N_M^2).$$

We conclude that for small N_M, the eigenvalues are approximately equal to those of the 2×2 submatrix $\boldsymbol{A}_1$.

Suppose more generally that the natural frequencies Ω_k, Ω_{k+1} lie close together. Using the approximate theory we find that for small N_M these frequencies will be perturbed to

$$\omega_k^2, \omega_{k+1}^2 = \tfrac{1}{2}[\Omega_k^2 + \Omega_{k+1}^2 - N_M \Gamma_S \pm \Delta^{\frac{1}{2}}],$$

where the discriminant Δ is given by

$$\Delta = (\Omega_{k+1}^2 - \Omega_k^2)^2 - 2N_M(\Omega_{k+1}^2 - \Omega_k^2)\Gamma_D + N_M^2[\Gamma_D^2 + 4\Gamma_P], \tag{5.2}$$

and we have abbreviated,

$$\Gamma_S = \Gamma_{kk} + \Gamma_{k+1,k+1}, \quad \Gamma_D = \Gamma_{k+1,k+1} - \Gamma_{kk}, \quad \Gamma_P = \Gamma_{k,k+1}\Gamma_{k+1,k}.$$

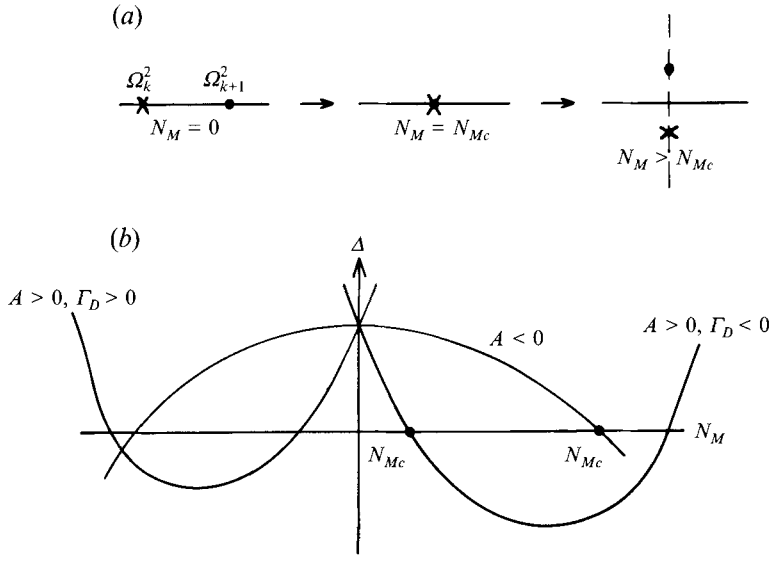

FIGURE 3. (*a*) Coalescence of eigenvalues and bifurcation into the complex plane. (*b*) Possible forms for the graph of Δ versus N_M.

The eigenvalues coalesce when $\Delta = 0$, i.e. when

$$N_M = \frac{\Omega_{k+1}^2 - \Omega_k^2}{\Gamma_D \pm 2(-\Gamma_P)^{\frac{1}{2}}}, \tag{5.3}$$

so coalescence occurs only if

$$\Gamma_P \leqslant 0. \tag{5.4}$$

When (5.4) is satisfied there are three possible forms for the graph of Δ versus N_M, illustrated in figure 3(*b*). If the coefficient of N_M^2 in (5.2),

$$\Gamma_D^2 + 4\Gamma_P = A \quad \text{say},$$

is negative the roots (5.3) have opposite sign. Since N_M is positive by definition we are concerned with only positive roots, and the plus sign must be chosen in (5.3). If on the other hand $A > 0$ there are two possibilities. If $\Gamma_D < 0$ both roots are negative and no bifurcation occurs; otherwise both roots are positive and bifurcation occurs at the root given by the positive sign in (5.3). Curiously, in the latter case, restabilization occurs at a higher value of N_M.

To summarize, complex bifurcation and instability occur if

$$[\Gamma_P < 0] \quad \text{and} \quad [(A < 0) \quad \text{or} \quad (A > 0 \quad \text{and} \quad \Gamma_D > 0)]. \tag{5.5}$$

The critical value of N_M for onset of instability is

$$N_{Mc} = \frac{\Omega_{k+1}^2 - \Omega_k^2}{\Gamma_D + 2(-\Gamma_P)^{\frac{1}{2}}}. \tag{5.6}$$

6. Results

In this section we examine the effects of various cell parameters on stability. In all calculations we took a cryolite depth of 5 cm, an aluminium pool depth of 20 cm, and considered only the first 12 modes (see figure 6). Exact eigenvalues of the interaction matrix were computed using the NAG routine F02AFF.

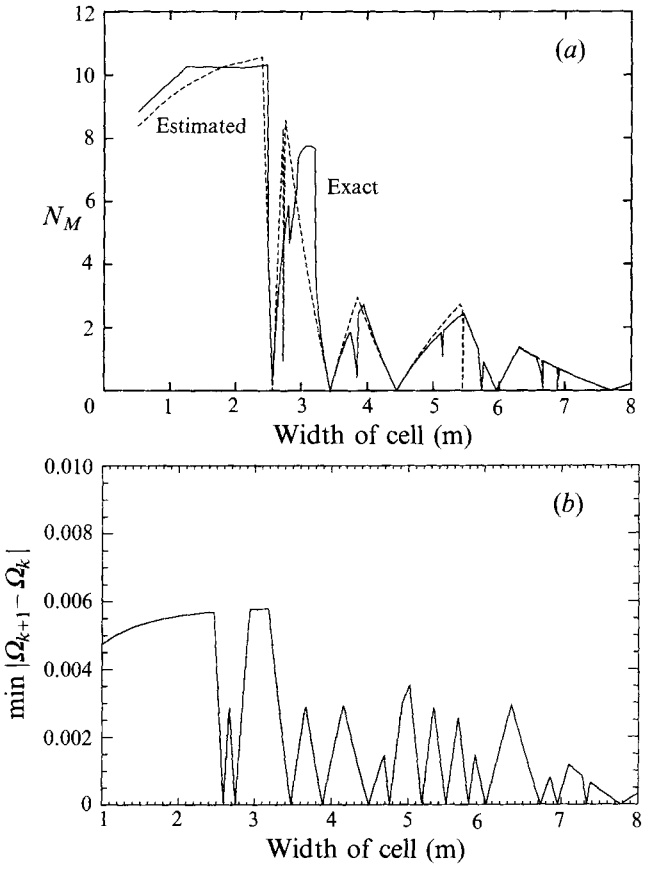

FIGURE 4. (*a*) Comparison of estimated and exact values of N_{Mc}. (*b*) Graph of minimum natural frequency separation versus cell width b. In both diagrams the cell length $a = 7.7$ m, $h_1 = 0.2$ m, $h_2 = 0.05$ m. In (*a*) $B_{0z}/\mu_0 J_0 a = 0.026$, $B_{0x} = B_{0y} = 0$, $q = 1$ and $\beta = 90°$.

Figure 4(*a*) compares exact values of N_{Mc} obtained by computing the eigenvalues of the full matrix, with estimates based on the approximate methods described in §5. The estimate of N_{Mc} is the value given by (5.6) minimized over all adjacent frequency pairs (the minimum usually occurring at the frequency pair that is closest together for $N_M = 0$).

Figure 4(*b*) shows a graph of the minimum natural frequency separation for a rectangular cell (taken over the first 12 modes) versus width b for a cell of fixed length $a = 7.7$ m. Aspect ratios where two natural gravity-wave frequencies coincide could be called *critical*, since such cells may be very easily destabilized. Figure 4(*b*) shows fourteen such critical aspect ratios but in figure 4(*a*) there are only eight values of b at which $N_{Mc} \to 0$. The remaining six (for example $b \approx 3.9$) correspond to the case $A > 0, \Gamma_D < 0$ illustrated in figure 3, and no transition to instability is predicted by either the exact calculations or approximate theory. However, an instability 'spike' appears to be drawn down from the exact graph.

Generally our estimated N_{Mc} is quite accurate, particularly near critical aspect ratios where destabilization occurs principally via a two-mode interaction. It is less accurate when the cell is very stable and many modes must combine to effect instability. At one critical aspect ratio ($b = 5.5$) our approximate method predicts transition to instability

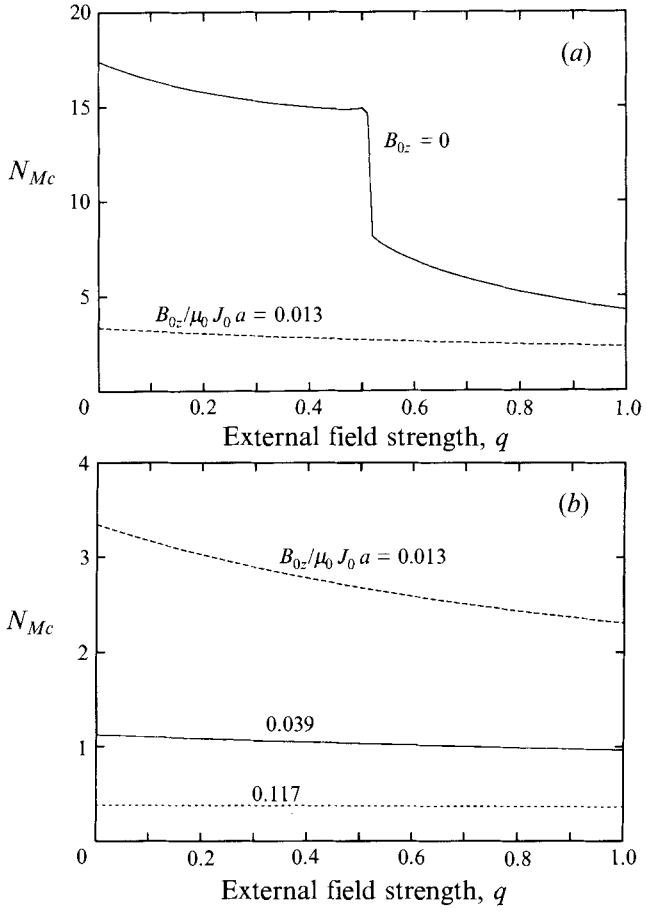

FIGURE 5. Graphs of N_{Mc} versus q (the external horizontal magnetic field strength) for various values of the dimensionless vertical magnetic field $B_{0z}/\mu_0 J_0 a$. Other cell parameters have the following fixed values: $a = 7.7$ m, $b = 4.0$ m, $B_{0x} = B_{0y} = 0$, $h_1 = 0.2$ m, $h_2 = 0.05$ m, $\beta = 90°$.

but the exact calculation does not. The instability predicted by the approximate two-mode analysis is very weak, and is overwhelmed when the effects of other modes are taken into consideration.

To emphasize one of the main points of this paper – if any two natural gravity-wave frequencies are nearly equal only a very small electromagnetic force is necessary to destabilize the system. There is a resonant interaction between the two modes, the Lorentz-force perturbation due to each one energizing the other. The physics of the resonance is complicated, depending on cell geometry and the details of the local and far fields, but the mechanisms would be similar to that described in paper II. Cells should be designed therefore with an aspect ratio aimed at keeping the eigenvalues λ_n, and hence the natural frequencies, as far apart as possible. From figure 4(*b*) it appears that an aspect ratio of about 7.7/3.0 maximizes frequency separation, but as we have seen, not all potential resonances actually lead to instability.

In figure 5 we examine the effect of the far-field strength, plotting N_{Mc} versus q for various values of B_{0z}. Generally the trend of the graphs is downwards with increasing q, showing – as one would expect – that increasing the external magnetic field makes the cell more unstable. When $B_{0z} = 0$ the graph is discontinuous at $q \approx 0.5$ where destabilization via a second and closer frequency pair first becomes possible. Clearly

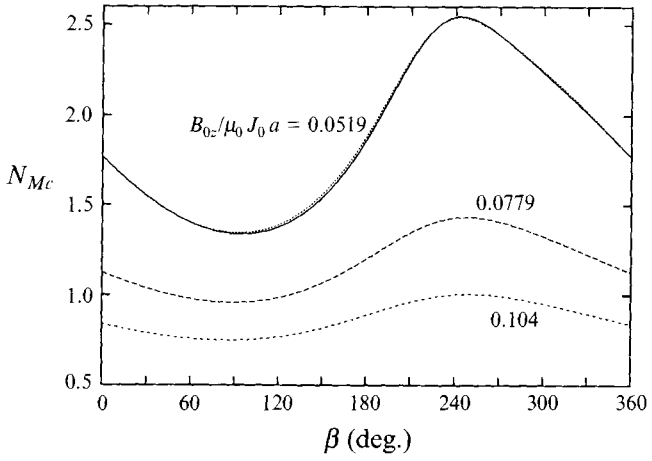

FIGURE 6. Graphs of N_{Mc} versus β (the angle between the principal axis of the far field and the major cell axis) for various values of $B_{0z}/\mu_0 J_0 a$. The solid curve $B_{0z}/\mu_0 J_0 a = 0.0519$ was computed with $N = 12$, i.e. with a 12-mode truncation level, and the adjacent dotted curve with $N = 24$. For the other curves the two truncation levels give indistinguishable results.

however the influence of B_{0z} is predominant – the critical value of N_M decreasing rapidly as the vertical field increases.

In figure 6 we plot N_{Mc} versus β – the angle between the principal axis of the external magnetic field, and the x-axis, or major cell axis. The cell is most stable when the principal axis, or symmetry axis of the external field, is inclined at an angle of 270° to the longer cell wall, and most unstable when this angle is 90°. It is not surprising that there exists such a marked lack of reflectional symmetry, given that $\boldsymbol{B}$ is a pseudo vector (Moffatt 1978). This figure also provides justification for the 12-mode truncation level. The dotted curve adjacent to the solid curve ($B_{0z}/\mu_0 J_0 a = 0.0519$) was calculated using a 24-mode truncation level, and clearly the results differ only slightly. For the other two curves the results are indistinguishable.

It is interesting to compare our results with those obtained from previous calculations based on a single Fourier mode. For example paper II predicts that instability will occur when

$$\frac{\mu_0 J_0^2 L^2}{h_2 g \Delta\rho} = N_M \frac{h_1}{L} = O(1) \quad \text{or} \quad N_M \approx \frac{h_1}{L} \approx 10^{-1}.$$

Our results generally predict instability when $N_M = O(1)$ (as our order-of-magnitude analysis would suggest) and the presence of cell walls therefore seems stabilizing. However, when two natural frequencies are weakly separated it is clear from (5.6) and figure 4(a, b) that instability can occur for arbitrarily small N_M via a two-mode resonance. Moreover, even when the natural frequencies are well separated, the vertical magnetic field can destabilize the cell when $N_M = O(10^{-1})$ (figure 5). Generally our stability predictions seem consistent with the single Fourier component models, but mode resonance is a new feature.

In all the above results, N_{Mc} is taken as the *smallest* value of N_M for the onset of instability. As pointed out in §5 our approximate theory predicts that the cell may restabilize as N_M is further increased. This curious feature has also been noticed in our exact numerical calculations, but these always predict a further eventual destabilization by a different mode pair. These isolated stability bands which thus occur in an unstable region are usually quite narrow.

7. Conclusions

In this paper we have developed a normal mode stability analysis for interfacial waves in an aluminium reduction cell. Such waves consist essentially of a combination of gravity modes weakly coupled by electromagnetic effects. Our most significant conclusion is that previous stability theories which analyse a single Fourier component wave are incomplete. The heterogeneous magnetic field links the evolution of different modes, which may thereby destabilize one another. In particular, if two modes have similar frequencies they may interact resonantly to destabilize the cell at quite small current values.

Stability is determined by calculating the eigenvalues of an interaction matrix which, in general, might be time-consuming to compute. However, an approximate method of analysis is available which involves calculation of only the three main diagonals or, when two natural frequencies are almost equal, only a 2×2 submatrix. This approximation seems accurate unless the cell happens to be particularly stable.

Our results show that cells become more unstable as the external field increases. An order-of-magnitude analysis shows that the vertical field component is particularly dangerous, and this is confirmed by detailed calculations. Cells are most stable when the symmetry axis (or principal axis) of the external field makes an angle of 270° with the major cell axis, and most unstable when this angle is 90°.

Although our model cell is very simple and somewhat unrealistic, the method can be generalized to deal with cells of arbitrary shape, and general magnetic fields. One complication we have avoided (by means of the simple vertical current distribution) is that in general the cryolite and aluminium layers will be moving, possibly with different velocities. This means motion would need to be calculated and a Kelvin–Helmholtz instability incorporated into the analysis. A more realistic treatment should also include damping due to fluid or turbulent viscosity, and to induced currents.

In the course of this work A.W. was supported by a Comalco Doctoral Scholarship. We also acknowledge many useful discussions with David Billinghurst and other staff of the Comalco Research Centre, Melbourne, Australia.

Appendix. Expressions for integrals

This Appendix gives explicit expressions for the integrals (4.18):

$$I^{(0)}_{kn} = \frac{1}{\lambda_k(\lambda_k^2-\lambda_n^2)}[\lambda_k(1+\mathscr{C}_{n2}\mathscr{C}_{n1})+\lambda_n(\mathscr{S}_{k2}\mathscr{S}_{n2}-\mathscr{C}_{k2}\mathscr{C}_{n2}-\mathscr{C}_{k1}\mathscr{C}_{n2})], \quad k\neq n,$$

$$I^{(0)}_{kk} = \frac{1}{2\lambda_k^2}(1+\mathscr{C}_{k2}\mathscr{C}_{k1}+\mathscr{C}_{k2}\mathscr{S}^2_{k1}h_1\lambda_k),$$

$$I^{(2)}_{kn} = \frac{\lambda_k}{\lambda_k^2-\lambda_n^2}[\mathscr{C}_{n2}(\mathscr{C}_{k1}\mathscr{C}_{n1}-\mathscr{S}_{k1}\mathscr{S}_{n1})-\mathscr{C}_{k2}], \quad k\neq n, \quad I^{(2)}_{kk} = \tfrac{1}{2}h_2\mathscr{S}^2_{k2};$$

$$I^{(1)}_{kn} = \frac{-\lambda_n^2}{\lambda_k^2}I^{(2)}_{kn},$$

where $\mathscr{S}_{ki} = \operatorname{cosech}(\lambda_k h_i)$.

In the case of the rectangular cell the eigenfunctions are most naturally labelled by a pair of integer subscripts:

$$E_{mn} = \cos(m\pi x/a)\cos(n\pi y/b).$$

We also introduce the symbol

$$\sigma_{mp} = \begin{cases} 0 & \text{if } m+p \text{ is even;} \\ 2 & \text{if } m+p \text{ is odd;} \end{cases}$$

where m and p are integers.

$$I^{(3)}_{mnpq} = \int_S (\nabla E_{mn} \times \nabla E_{pq}) \cdot \hat{z}\, \mathrm{d}x\, \mathrm{d}y = \sigma_{mp}\sigma_{nq} \frac{m^2q^2 - p^2n^2}{(m^2-p^2)(q^2-n^2)}, \quad m \neq p \text{ and } n \neq q.$$

Otherwise $I^{(3)}_{mnpq} = 0$.

$$I^{(4)}_{mnpq} = \frac{\sigma_{mp}\sigma_{nq}}{\pi^2}\left[\frac{a^2\alpha_{11}\, q^2(m^2+p^2)}{(m^2-p^2)^2(n^2-q^2)} - \frac{b^2\alpha_{22}\, p^2(n^2+q^2)}{(m^2-p^2)(n^2-q^2)^2}\right],$$

provided $m \neq p$ and $n \neq q$.

$$I^{(4)}_{mnmq} = \frac{aq^2(1+\delta_{m0})}{2(q^2-n^2)}[\sigma_{nq}(B_{0x} + \tfrac{1}{2}\alpha_{11}\, a) - \alpha_{12}\, b(-1)^{n+q}],$$

$$I^{(4)}_{mnpn} = \frac{-bp^2(1+\delta_{n0})}{2(p^2-m^2)}[\sigma_{mp}(B_{0y} + \tfrac{1}{2}\alpha_{22}\, b) - \alpha_{21}\, b(-1)^{m+p}].$$

Finally, $$I^{(4)}_{mnmn} = \tfrac{1}{8}ab[(1+\delta_{n0})(1-\delta_{m0})\,\alpha_{21} - (1+\delta_{m0})(1-\delta_{n0})\,\alpha_{12}].$$

REFERENCES

DESCLOUX, J., FLUECK, M. & ROMERIO, M. V. 1991 Modelling for instabilities in Hall–Héroult cells: mathematical and numerical aspects. In *MHD Process Metallugry*. The Minerals, Metals and Materials Society.

LYMPANY, S. D., EVANS, J. W. & MOREAU, R. 1983 Magnetohydrodynamic effects in aluminium reduction cell. In *Proc. IUTAM Symp. on Metallurgical Applications of Magnetohydrodynamics, Cambridge, 1982*, pp. 15–23. London: The Metals Society.

MOFFATT, H. K. 1978 *Magnetic Field Generation in Electrically Conducting Fluids*. Cambridge University Press.

MOREAU, R. & ZIEGLER, D. 1986 Stability of aluminium cells: a new approach. *Light Metals*, pp. 359–364.

PIGNY, S. & MOREAU, R. 1991 Stability of fluid interfaces carrying an electric current in the presence of a magnetic field. *Euro. J. Mech.* B **11**, 1–20.

POTOČNIK, V. 1989 Modelling of metal-bath interface waves in Hall–Héroult cells using ESTER/PHOENICS. *Light Metals*, pp. 227–235.

SNEYD, A. D. 1985 Stability of fluid layers carrying a normal electric current. *J. Fluid Mech.* **156**, 223–236 (referred to herein as paper I).

SNEYD, A. D. 1992 Interfacial instabilities in aluminium reduction cells. *J. Fluid Mech.* **236**, 111–126 (referred to herein as paper II).

URATA, N. 1985 Magnetics and metal pad instability. *Light Metals*, pp. 581–589.